CHEMISTRY OF MATERIALS

ARTICLE

pubs.acs.org/cm

Porous Pd Layer-Coated Au Nanoparticles Supported on Carbon: Synthesis and Electrocatalytic Activity for Oxygen Reduction in Acid Media

Jun Ho Shim,[‡,§] Jiyoung Kim,[‡,§] Chongmok Lee,[*,§] and Youngmi Lee[*,§]

[§]Department of Chemistry and Nano Science, Ewha Womans University, Seoul 120-750, Korea

ABSTRACT: This paper reports the simple synthesis and characterization of carbon-supported Pd layer-coated Au nanoparticles (AuPd/C). A series of AuPd/C with various Pd/Au weight percentage ratios were prepared by the spontaneous deposition of a Pd shell on a Au nanoparticle core using different Pd precursor concentrations (0.5, 5, 10, 20 mM $PdCl_2$). Au nanospheres encapsulated by the porous Pd shells are confirmed by transmission electron microscopy (TEM), UV−vis absorption spectroscopy, and scanning TEM. The catalytic activity of the AuPd/C for the oxygen reduction reaction (ORR) was investigated by rotating disk electrode voltammetry in 0.5 M H_2SO_4. In particular, a AuPd/C with a Pd/Au ratio of 0.61 shows superior ORR activity along with satisfactory stability and methanol tolerance under acidic conditions.

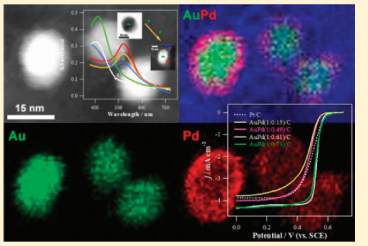

KEYWORDS: gold, palladium, spontaneous deposition, bimetallic nanoparticle, core−shell, oxygen reduction reaction

INTRODUCTION

Efficient electrocatalysts are desired in many electrochemical fields. In particular, the development of a fuel cell cathode catalyst for the oxygen reduction reaction (ORR) is recognized as one of the most important research areas because the generated energy efficiency in a fuel cell is decreased mainly by the sluggish ORR, requiring a high overpotential. Although Pt or Pt-based electrocatalysts are the most commonly used cathode catalysts in fuel cells due to the high activity of Pt for the ORR, the high cost and limited supply of Pt have prompted a search for new efficient catalysts with a low Pt content or without Pt. To improve the catalytic activity with a lower Pt loading, some methods for trimming the metal morphology on the nanometer scale, such as nanoparticles (NPs) resulting in the increased active surface area[1−3] and alloying Pt with other metals,[4,5] have been employed. A study of non-Pt electrocatalysts has also been attempted. For example, nanostructured materials based on relatively less expensive transition metals (e.g., Pd),[6,7] surface modified nanometer sized carbon (e.g., nitrogen-doped carbon nanotubes),[8,9] and a combination of them[10] are commonly found.

Being a more economic and plentiful metal than Pt, Au has been investigated for its electrocatalytic activity. On the other hand, the weak chemisorption properties of Au due to the filled d-band result in low catalytic activity.[11−13] The current strategy to improve the activity relies mainly on the increase in surface to volume ratio by employing NPs or highly porous structures and a surface coating or alloys with foreign metals. Catalysts based on pure Au, however, still show lower activity particularly for the ORR compared to Pt-based ones. Therefore, Pt is commonly chosen as a coating metal or alloying partner for Au to achieve the relevantly improved activity. Indeed, the alloyed AuPt NPs were reported to show high catalytic activity toward the ORR[14,15] and methanol oxidation reaction (MOR).[16,17] More recently, Au cluster-coated Pt NPs[18] and Pt deposits on Au NPs produced using spontaneous deposition method[19] were evaluated for their impact on the ORR and formic acid oxidation, respectively. The synthesis of a sponge-like Au/Pt core/shell electrocatalyst with a hollow cavity using a modified galvanic replacement reaction (GRR) and its enhanced activity for the ORR and MOR were also reported.[20]

Pd has also attracted considerable attention because it has very similar properties to Pt (e.g., same group of the periodic table, same fcc crystal structure, and similar atomic size) while being less expensive and more abundant than Pt.[21] Indeed, many Pd-based electrocatalysts have been studied intensively in recent years, as one of the most promising Pt-free catalysts. Considering the great similarity between Pd and Pt, a class of Au catalysts coated or alloyed with Pd instead of Pt has been introduced. For example, Pd-coated nanoporous Au[22] and nanoporous Au−Pd alloys[23] were synthesized and examined for the ORR and MOR, respectively. In addition, the enhanced catalytic activities of Pd coated Au NPs for ethanol oxidation[24] and a Au/Pd core shell with a hollow cavity for methanol, ethanol, and formic acid oxidation were reported under alkaline conditions. On the other hand, these catalysts required rather complicated synthetic procedures, as follows: underpotential deposition of a sacrificial Cu layer on nanoporous Au and subsequent replacement with Pd;[22] production of multicomponent metallic glass followed by dealloying;[23] Pd precursor reduction on a nanostructured Au template using reducing agent (e.g., ascorbic acid);[24,25] etc. Moreover, the activity of these Au−Pd bimetallic catalysts has

Received: April 27, 2011
Revised: September 14, 2011
Published: October 04, 2011

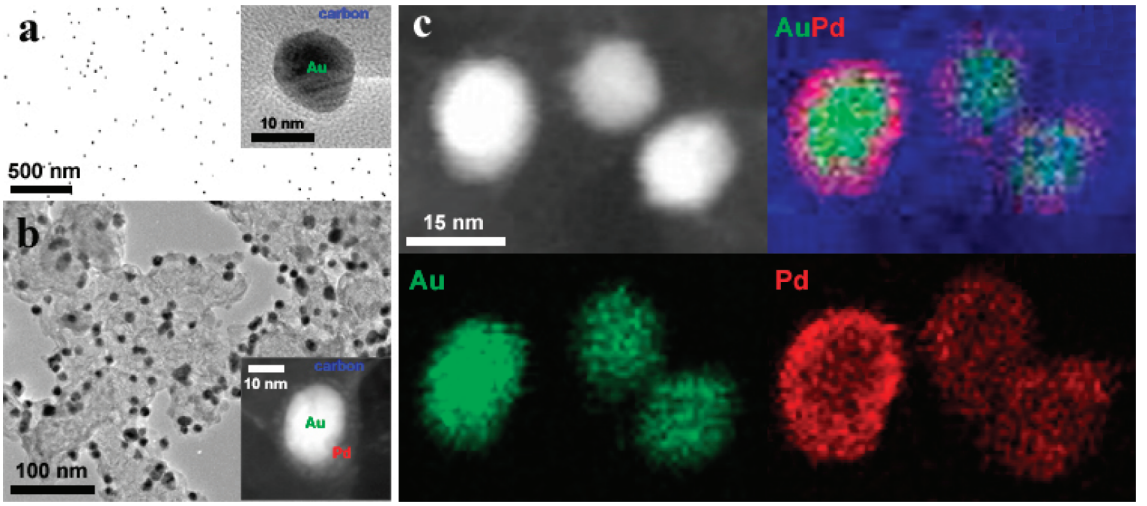

Figure 1. TEM images of (a) Au NPs and (b) AuPd(1:0.61)/C nanoparticles synthesized by a spontaneous reduction reaction. The inset (a and b) shows the corresponding a magnified TEM image of a single Au NP on carbon and a HAADF-STEM image of a AuPd(1:0.61)/C, respectively. (c) Representative HAADF-STEM image (top left panel) of the AuPd(1:0.61)/C and its corresponding Pd (red) and Au (green) elemental mapping image. The blue color of the top right panel corresponds to carbon support of the AuPd(1:0.61)/C.

been reported in neutral or alkaline conditions presumably due to the relatively low stability of Pd under acidic conditions.[26] More recently, the synthesis of two different types of Pd−Au bimetallic nanocrystals depending on the kind of reducing agent was reported though their catalytic activity was not studied.[27]

This paper reports a simple synthetic method of carbon-supported Pd-coated Au NPs (denoted as AuPd/C) via the spontaneous reduction of Pd(II) to Pd on a Au NP surface without a treatment with any additional reducing agent. The catalytic activity toward the ORR and the tolerance to methanol of the prepared catalysts in a 0.5 M H_2SO_4 solution were investigated as a function of the Pd/Au composition ratios. The results revealed sufficient stability in acidic media.

EXPERIMENTAL SECTION

Materials. Hydrogen tetrachloroaurate trihydrate ($HAuCl_4•3H_2O$), sodium citrate ($Na_3C_6H_5O_7•3H_2O$), 5.0 wt% Nafion, and potassium hexacyanoferrate ($K_3[Fe_3(CN)_6]$) were purchased from Sigma Aldrich (St. Louis, MO). Palladium chloride ($PdCl_2$) and carbon black were obtained from Alfa Aesar (Ward Hill, MA). Sulfuric acid (H_2SO_4) and perchloric acid ($HClO_4$) used as electrolytes were supplied by Dae Jung Co. (Korea). Potassium chloride (KCl) was received from Duksan Co. (Korea). Commercial Pt/C (20 wt % Pt loading on carbon Vulcan XC-72) catalyst was a product of E-TEK. Methyl alcohol was acquired from Hayman (Witham, Essex, UK). All solvents and chemicals were of analytical-reagent grade, and the solutions were prepared using 18 MΩ cm^{-1} deionized water.

Preparation of Carbon-Supported Au/C Catalyst. Au NPs were synthesized using a similar method to the one described previously.[28] First, 20 mL of a 1.0 mM $HAuCl_4$ aqueous solution was heated to boil, and 2 mL of 38.8 mM citrate solution was added to this boiling solution with vigorous stirring. The color of the solution was changed gradually to a light yellow, purple, and then deep red color. When it became a deep red color, stirring was stopped, and the solution was kept under dark conditions prior to use. The solution of Au NPs was mixed with a carbon support dispersed in water (2.0 mg mL^{-1}) by stirring for 5 h. The resulting carbon supported Au NPs (Au/C) were filtered and washed thoroughly with distilled water. The Au/C was separated from the washing water by centrifugation at 4000 rpm for 20 min. This washing step was repeated at least three times. The thoroughly washed Au/C settled at the bottom of the centrifuge cell was then dried completely overnight under vacuum environment.

Spontaneous Deposition of Pd on Au NPs. AuPd/C was prepared as follows. A mixed solution of Au/C was dispersed in water (1 mg mL^{-1}) and added to a $PdCl_2$ solution at various concentrations (0.5, 5, 10, and 20 mM). The resulting mixture was stirred for 5 h at room temperature, resulting in Pd thin layer deposition on the surface of the Au NPs. The prepared AuPd/C in a suspension was filtered and washed thoroughly with distilled water to remove the unreacted Pd precursor. The AuPd/C catalysts were dried completely under a vacuum environment overnight and kept in a refrigerator prior to use.

Electrocatalyst Characterizations. High-resolution transmission electron microscopy (HR-TEM; JEOL JEM-3010, 300 kV) images were obtained to verify the surface morphology and composition of the synthesized catalysts. The elemental mapping images were taken using a FEI Tecnai F20 scanning transmission electron microscope (STEM). The UV−vis spectra of the Au/C and AuPd/C hydrosols were obtained with a HP-8452A spectrophotometer equipped with quartz cells. The atomic ratios of the AuPd/C catalysts were analyzed by energy dispersive X-ray spectroscopy (EDS) integrated with a scanning electron microscope (SEM; Jeol JSM-6700F).

Electrochemical Measurements. A glassy carbon (GC) disk electrode surface (diameter = 3 mm, Bioanalytical Systems, Inc. (BAS)) was loaded with Pt/C, Au/C, and AuPd/C catalysts independently as follows. First, each catalyst suspension was prepared by mixing the catalyst in deionized water (2.0 mg mL^{-1}). Ten μL of the suspension was applied to a GC disk by pipetting and dried. These steps were repeated three times. Subsequently, 10 μL of a Nafion solution (0.05 wt%) was applied over the dried electrode and then dried at ambient temperature. A bulk Pt electrode (diameter = 3 mm, BAS) was also used for comparison. The activity of the prepared catalysts for ORR was characterized by rotating disk electrode (RDE) voltammetry. All electrochemical experiments were carried out using a RDE-1 rotor and BAS 100 B/W electrochemical analyzer (BAS) with a saturated calomel reference electrode (SCE, 0.241 V vs NHE) and Au wire counter electrode to prevent possible Pt contamination. The RDE experiments were run in a 0.5 M H_2SO_4 aqueous solution saturated with either oxygen or nitrogen (Dong-A gas Co.) at scan rate of 10 mV s^{-1}. Cyclic voltammetry (CV) was carried out using a 900B bipotentiostat (CH

dx.doi.org/10.1021/cm2012044 |Chem. Mater. 2011, 23, 4694–4700

Instrument, Inc.). The measured currents were converted to a current density by normalization to the geometric surface area (GSA) of each modified electrode which was determined by chronocoulometry (CC) in a 10 mM $K_3Fe(CN)_6$ aqueous solution containing 0.1 M KCl as the supporting electrolyte.

RESULTS AND DISCUSSION

Characterizations of AuPd/C. The morphology and size of the prepared Au NPs and AuPd/C were characterized by TEM. Figure 1a shows a typical TEM image of the Au NPs before (main) and after (inset) loading on the carbon support, confirming the almost spherical shape and narrow size distribution of the Au NPs (ca. 13 nm in diameter). Once loaded, the Au NPs were well dispersed on the carbon support without changes in the size distribution (not shown). After the spontaneous deposition of Pd on the Au NPs, the resulting AuPd NPs were also evenly dispersed within the carbon support with negligible agglomeration, similar to the parent Au NPs (Figure 1b). No noticeable size differences were observed between the Au NPs and AuPd NPs (insets of Figure 1a and b), indicating that spontaneous Pd layer deposition was associated with Au NP etching. In other words, a Pd coating on a Au NP core appears to occur presumably via a GRR-like mechanism. Considering the slightly more positive standard reduction potential of Au(III) ($AuCl_4^-$/Au, +1.002 V vs NHE) than the one of Pd(II) (Pd^{2+}/Pd, 0.951 V vs NHE),[29] a GRR between Au and Pd(II) (eq 1) is not anticipated to be favorable. AuPd NPs can only be produced when the chloride ion concentration is rather high. On the other hand, the wt% ratios of Pd/Au estimated by SEM-EDS suggest quite favorable Pd layer deposition on Au core. Indeed, the averaged Pd/Au wt% ratios (from measurements at 10 different locations of each catalyst) increased with increasing Pd precursor concentrations as follows: 0.15 ± 0.06, 0.49 ± 0.08, 0.61 ± 0.11, and 0.73 ± 0.11 for 0.5, 5, 10, and 20 mM $PdCl_2$, respectively.

For the rest of this paper, a series of as-prepared AuPd/C catalysts are denoted as AuPd(Au:Pd wt% ratio)/C based on their composition. In addition, ΔPd (increase in Pd) to −ΔAu (decrease in Au) was approximately 1.5:1, which is in good agreement with GRR ratio between Au/Au(III) and Pd(II)/Pd, particularly when the Pd precursor concentration was ≥10 mM. On the other hand, the replacement molar ratios of Au(III)/Pd were determined to be >1.5 when the Pd precursor concentration was low, i.e., ~3.5 (0.5 mM $PdCl_2$) and ~2.4 (5 mM $PdCl_2$), suggesting other processes in addition to the GRR, such as underpotential deposition, are involved in Pd layer formation. One possible reason for the observed favorable GRR-like Pd deposition associated with Au etching, in contrast to the thermodynamic expectation from the reduction potentials, could be the adsorption of chloride (from $PdCl_2$) on the Au NP surface,[30] inducing an increase in the local chloride concentration and therefore facilitating Au oxidation to $AuCl_4^-$ and Pd^{2+} reduction by shifting the equilibrium to the right side in eq 1. Recently, similar synthesis of Pd−Pt bimetallic nanocrystals and Pd−Pt nanodendrites for ORR has been reported by the Xia group.[31,32] Nevertheless, further study will be needed to clarify the mechanism of AuPd NP formation

$$3Pd^{2+}(aq) + 2Au(s) + 8Cl^-(aq) \leftrightarrow 3Pd(s) + 2AuCl_4^-(aq) \quad (1)$$

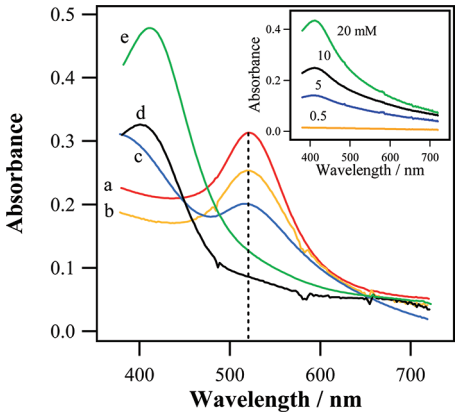

Figure 2. Representative UV−visible spectra of hydrosols containing the NPs of (a) Au, (b) AuPd (0.5 mM $PdCl_2$), (c) AuPd (5 mM $PdCl_2$), (d) AuPd (10 mM $PdCl_2$), and (e) AuPd (20 mM $PdCl_2$). The dotted line indicates the maximum SPR of gold colloid at 520 nm. The inset shows the absorption spectra for the $PdCl_2$ aqueous solutions.

The averaged wt% of the total Au and Pd determined by EDS was ca. 10% for all catalysts prepared.

The deposited Pd layer was not readily distinguished from the Au core in the TEM images, possibly suggesting epitaxial growth of the Pd layer on the Au NP surfaces. On the other hand, high-angle annular dark-field scanning TEM (HAADF-STEM) analysis distinctively revealed the Au nanosphere core and surrounding Pd shell. Indeed, a close inspection of a single AuPd(1:0.61) NP supported on C in the HAADF-STEM image enabled a brighter core to be distinguished from the darker shell (inset of Figure 1b). This suggests that the NPs are composed of a shell containing a lighter element (Pd) than the core (Au) because the contrast variations in HAADF-STEM are proportional to the square of the element atomic number. The darker shell could be also ascribed to more porous structure than the brighter core (as shown in change of surface area confirmed by CV, *vide infra*). Elemental mapping of Au and Pd shows more clearly that the AuPd NP structures constituted with Au core are fully encapsulated with a uniformly deposited Pd thin layer shell (Figure 1c).

The NPs were further analyzed by UV−vis absorption spectroscopy. In addition to TEM analysis, the size of the parent Au NPs was estimated successfully from the UV−vis absorption spectra. Strong absorption at ~520 nm was observed for the Au NP colloidal solution due to the surface plasmon resonance (SPR) of the Au NPs prepared with citrate reductase (Figure 2a). The color of the solution containing Au NPs depends on the size and shape of the NPs. Absorption peak at 520 nm is well correlated with the Au NP size (ca. 13 nm) determined in TEM image. On the other hand, the Au SPR at 520 nm was decreased accordingly for AuPd NPs as the Pd precursor concentration was increased and eventually disappeared when the Pd precursor concentration was ≥10 mM (Figure 2b-e). This shows that the Pd layer coats the Au NP core completely. The UV−vis spectra were obtained for a solution containing the NP catalysts and the remaining unreacted Pd precursor (Pd^{2+}) in the absence of a carbon support due to the interference of carbon with the UV−vis absorbance measurements and the difficulty in collection of the NPs without a carbon support from the solution. Therefore, the gradually increased absorption intensity at ~415 nm with increasing $PdCl_2$ concentration was attributed to Pd^{2+}. Indeed, the absorption spectra obtained for the solution

dx.doi.org/10.1021/cm2012044 |*Chem. Mater.* 2011, 23, 4694–4700

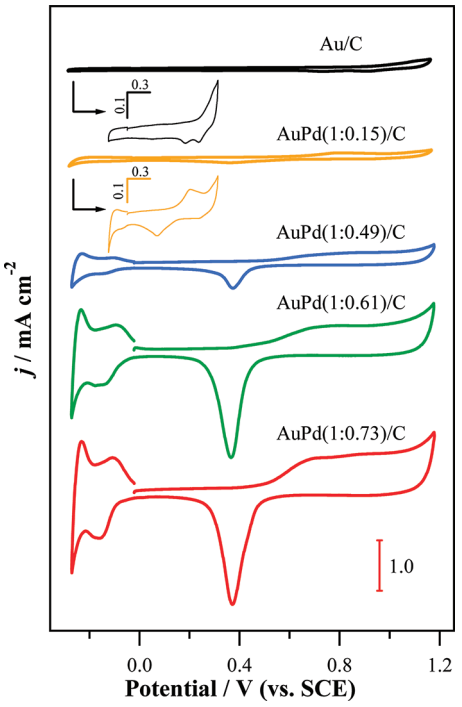

Figure 3. Cyclic voltammograms obtained with AuPd/C-modified GC electrodes in Ar-saturated 0.1 M $HClO_4$ solution at a scanning rate of 10 mV s^{-1}. The arrows show the enlarged voltammograms of the Au/C and AuPd(1:0.15)/C, respectively.

containing only $PdCl_2$ shows the increase in the absorption intensity proportional to the concentration (inset of Figure 2), showing that the absorption at ~415 nm in Figure 2c-e is due to the remaining Pd^{2+}.

The Au/C and AuPd/C catalysts were characterized electrochemically by CV in a 0.1 M $HClO_4$ solution. In this paper, all electrochemical results for the catalysts, including CV shown in Figure 3, were presented as current densities after normalization to the corresponding electrode GSA. The GSAs of the electrodes were estimated by CC performed in a 10 mM $K_3Fe(CN)_6$ solution containing 0.1 M KCl, as reported previously.[33] From the slopes of the linear plot of the measured charge in CC vs time$^{1/2}$, the GSAs were determined to be greater (ca. 0.080−0.110 cm^2 depending on the catalyst loadings) than that of the substrate GC electrode (0.071 cm^2). This suggests that the AuPd/C catalysts are loaded even over the insulator of the GC electrode, resulting in an increased GSA.

A normalized cyclic voltammogram obtained with each catalyst loaded GC electrode exhibits three distinctive regions: a double layer capacitive region, a hydrogen adsorption/desorption region, and a metal oxide formation/reduction region. In particular, capacitive background current densities between the hydrogen and oxide regions were observed to increase from Au/C to AuPd/C and further increase with increasing Pd:Au ratio in AuPd/C. Since the particle sizes estimated from the TEM images were not different regardless of the NPs, the change in the capacitive currents indicates a rather porous Pd layer on Au NP core, leading to an enlarged actual surface area.

The hydrogen adsorption/desorption, occurring at a more negative potential range than ~0.0 V, was not observed in Au/C. On the other hand, a well-defined hydrogen peak appeared at AuPd/C and increased with increasing Pd:Au ratio, supporting

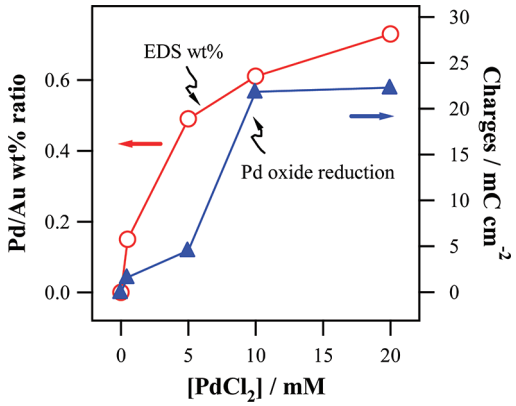

Figure 4. Plots of the Pd/Au wt% ratio (O) estimated by SEM-EDS and integrated reduction charge of surface Pd oxide (Δ) as a function of the precursor Pd concentration. The charge density was obtained by normalization to the GSA.

the successful deposition of a Pd shell on the Au core. Hydrogen adsorption on gold electrodes does not occur.[34] The anodic scan from 0.55 V corresponds to the formation of Pd surface oxides and finishes in the cathodic scan at 0.30 V for their reduction. For AuPd/C catalysts with higher Pd:Au ratio, the integrated charge amounts passed for the surface Pd oxide reduction (i.e., area under the cathodic peak at 0.39 V) became larger than those with a lower Pd:Au ratio. This suggests an increased Pd surface area, which is in agreement with the observation of capacitive current densities.

Figure 4 shows the Pd:Au wt% ratios and the charge amounts for surface Pd oxide reduction depending on the Pd precursor concentration regarding a series of AuPd/C catalysts. As described previously, the general tendency was an increase in both values with increasing precursor concentration. Although the Pd:Au ratio increased gradually, the charges corresponding to the Pd real surface area showed a rather small increase from 0.5 to 5 mM and a large increase, from 5 to 10 mM of $PdCl_2$. This suggests that the most efficient porosity of the Pd layer, which is possibly related to the catalyst activity, is achieved on the Au core at 10 mM among the precursor concentrations studied.

ORR at the Catalysts. The catalytic performance of Au/C and a series of AuPd/C catalysts toward the ORR were investigated by RDE voltammetry under acidic conditions. Figure 5 shows the normalized RDE voltammetric curves recorded in the O_2-saturated 0.5 M H_2SO_4 solution at 1600 rpm with each catalyst-loaded GC electrode. For comparison, a commercial Pt/C catalyst-loaded GC and bulk Pt disk electrodes were also studied for the ORR activity. The ORR began at slightly more positive potentials for AuPd(1:0.73)/C and Pt/C followed very closely by AuPd(1:0.61)/C. Indeed, the ORR onset potentials were more positive in the following order: AuPd(1:0.73) ≈ Pt/C > AuPd(1:0.61)/C > AuPd(1:0.49)/C ≈ AuPd(1:0.15)/C > bulk Pt ≫ Au/C. The trend of the half-wave potentials ($E_{1/2}$) was similar to that of the ORR onset potentials. One thing to note is that the $E_{1/2}$ value at AuPd(1:0.61)/C (0.53 V vs SCE; 0.771 vs NHE) was more positive than that at both AuPd(1:0.73)/C (0.52 V vs SCE; 0.761 vs NHE) and Pt/C (0.49 V vs SCE; 0.731 vs NHE). This is in contrast to the onset potential due to the much steeper RDE curve shape, indicating a rather faster ORR kinetics at AuPd(1:0.61)/C. The RDE curve sharpness in the mixed kinetic-diffusion controlled region was confirmed more clearly from the ΔE values for the middle 90% changes of the

dx.doi.org/10.1021/cm2012044 |*Chem. Mater.* 2011, 23, 4694–4700

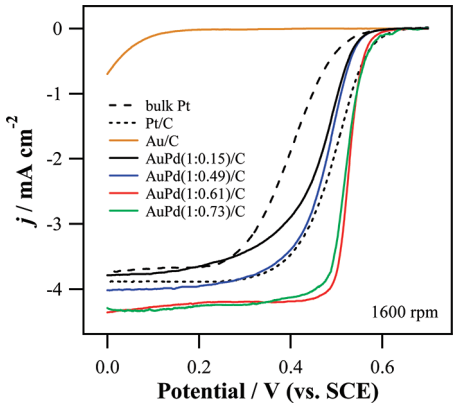

Figure 5. RDE voltammograms for oxygen reduction in an O_2-saturated 0.5 M H_2SO_4 at the bulk Pt, Pt/C, Au/C, AuPd(1:0.15)/C, AuPd(1:0.49)/C, AuPd(1:0.61)/C, and AuPd(1:0.73)/C electrodes at a scan rate of 10 mV s^{-1} with a rotation speed of 1600 rpm. The current density was obtained by normalization to the electrode GSA.

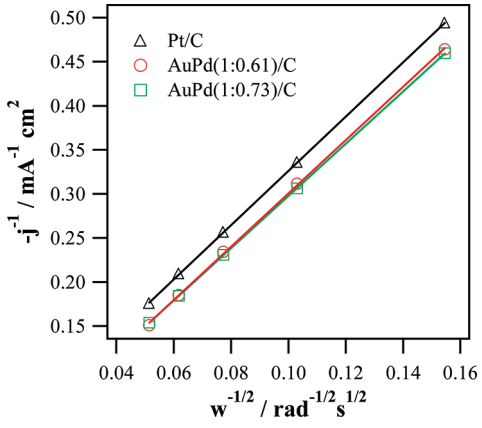

Figure 6. Koutecky–Levich plots for the oxygen reduction obtained from the RDE data presented in Figure 5: (Δ) Pt/C, (○) AuPd(1:0.61)/C, and (□) AuPd(1:0.73)/C.

limiting current densities (i.e., the smaller ΔE, the steeper the curve slope is): the measured ΔE values were 0.087 V for AuPd(1:0.61)/C; 0.15 V for AuPd(1:0.73)/C; and 0.22 V for Pt/C. In addition, similar diffusion-limited current densities, which were higher compared to the other catalysts, were observed at AuPd(1:0.61)/C and AuPd(1:0.73)/C. Indeed, the $E_{1/2}$ values at AuPd(1:0.61)/C and at AuPd(1:0.73)/C correspond to overpotentials of 0.415 and 0.425 V, respectively, from the thermodynamic O_2 reduction potential in the used experimental condition. The observed overpotentials at this AuPd/C catalyst system are comparable and/or superior to some other catalyst systems previously reported (e.g., mono-[35,36] or multinuclrear[37] non-noble metal complexes).

The number of electrons transferred (n) during the course of the ORR was calculated for two excellent AuPd/C catalysts (1:0.73 and 1:0.61) and commercial Pt/C from the RDE voltammetry results obtained at various electrode rotation speeds using the Koutecky–Levich (K-L) equation[38,39]

$$\frac{1}{j} = \frac{1}{j_k} + \frac{1}{j_d} = \frac{1}{j_k} + \frac{1}{0.62nFC_{O_2}D_{O_2}^{2/3}\nu^{-1/6}\omega^{1/2}} \qquad (2)$$

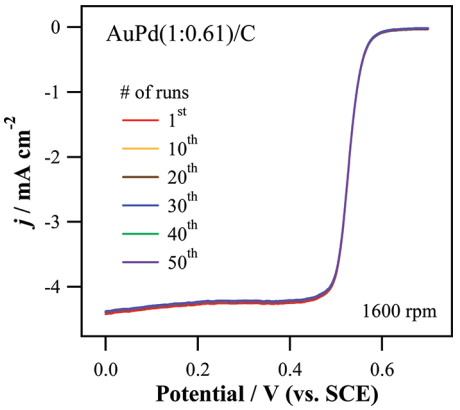

Figure 7. RDE voltammograms for the ORR obtained repetitively for 50 runs in an O_2-saturated 0.5 M H_2SO_4 solution using a AuPd(1:0.61)/C loaded GC electrode (scan rate of 10 mV s^{-1}).

where j is the overall current density, j_k is the kinetic current density, j_d is the diffusion current density, n is the number of electrons transferred in the ORR, F is the Faraday constant, C_{O_2} (1.1×10^{-6} mol cm^{-3}) is the saturated concentration of oxygen, D_{O_2} (1.4×10^{-5} cm^2 s^{-1}) is the diffusion coefficient of oxygen, ν is the kinematic viscosity of the solution (1.0×10^{-2} cm^2 s^{-1}), and ω is the electrode rotation rate. The parameters for the calculation were obtained from the literature.[40]

Figure 6 shows the K-L plots (j_d^{-1} vs $\omega^{-1/2}$) of the ORR using the RDE current densities at 0.10 V (vs SCE). The plots exhibit good linearity, indicating that the ORR kinetics is first order with respect to the reactant concentration. The calculated n values from the slope of the K-L plots for Pt/C, AuPd(1:0.61)/C, and AuPd(1:0.73)/C catalysts were 3.94, 4.01, and 4.09, respectively. The direct ORR pathway via 4-electron transfer is desirable rather than a 2-electron transfer pathway producing hydrogen peroxide, which might have an adverse effect on the stability of the catalysts. Indeed, 4-electron transfer ORR pathway, i.e., producing water as the main ORR product, is dominant in all three catalysts.

All aspects investigated (e.g., the ORR onset and half-wave potentials, the limiting current density levels, the RDE curve sharpness, and the n values) support the high ORR activity of AuPd/C (particularly with an optimized Au:Pd ratio = 1:0.61), even surpassing that of commercial Pt/C. The slightly better ORR catalytic activity of AuPd(1:0.61)/C even with a lower Pd content compared to AuPd(1:0.73) may be related to the efficient porosity of the Pd layer formed on Au, as described in the previous section (Figure 4). Moreover, almost identical RDE voltammograms, in terms of the ORR onset potential, curve shape, and limiting current, were obtained for at least 50 repeated RDE runs in an O_2 saturated 0.5 M H_2SO_4 solution, highlighting the satisfactory stability of the catalyst (Figure 7). The high ORR activity and high stability of AuPd(1:0.61)/C verified under acidic conditions are noteworthy features of AuPd/C catalysts, considering that most Au–Pd bimetallic catalysts has been reported elsewhere for their activity in neutral or alkaline conditions, presumably due to the low stability of Pd in acidic conditions.[26] When compared to the ORR activity of a few Pd based catalysts studied in acidic conditions, the AuPd/C catalyst system, in general, showed similar ORR onset potential, sharper RDE curve slope (i.e., faster kinetics), and higher stability.[41–45]

Methanol Tolerance at the Catalysts. When ORR catalysts are employed in the cathode of direct methanol fuel cells,

dx.doi.org/10.1021/cm2012044 |Chem. Mater. 2011, 23, 4694–4700

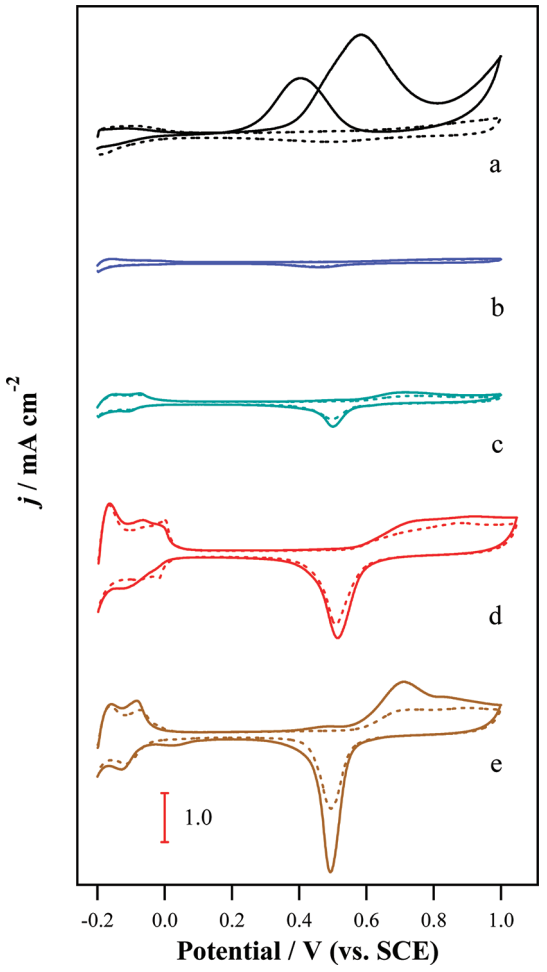

Figure 8. Cyclic voltammograms of the (a) Pt/C, (b) AuPd(1:0.15)/C, (c) AuPd(1:0.49)/C, (d) AuPd(1:0.61)/C, and (e) AuPd(1:0.73)/C catalysts recorded in a deaerated 0.5 M H_2SO_4 solution in the presence (solid line) and absence (dotted line) of 0.5 M methanol at a scan rate of 10 mV s^{-1}.

they generally suffer from a methanol crossover problem, which reduces the fuel cell efficiency. The tolerance to methanol was studied for the AuPd/C catalysts by performing CV in a deaerated 0.5 M H_2SO_4 solution. The commercial Pt/C showed the typical behavior of Pt metal in the presence of methanol, exhibiting anodic peak corresponding to methanol oxidation at ~0.58 V in the forward scan and another peak corresponding to the oxidation of adsorbed carbon species at ~0.40 V in the reverse scan (Figure 8a).[46] On the other hand, such oxidation peaks of methanol/carbon species were not pronounced at the AuPd/C catalysts (Figure 8b-e), i.e., remarkably higher tolerances to methanol were observed compared to the Pt/C catalyst. However, AuPd(1:0.73)/C showed a rather large current increase in the presence of methanol, suggesting the activity of a certain degree for the methanol oxidation. In fact, AuPd(1:0.61)/C, showing the highest ORR activity among the prepared AuPd/C catalysts, also exhibited best methanol tolerance (i.e., highest ORR selectivity in the presence of methanol), confirmed by very similar CVs in the presence or absence of methanol.

CONCLUSIONS

A series of carbon-supported Pd shell coated Au NPs were synthesized as a function of the Pd precursor concentration using a rather straightforward method. A porous Pd layer formed spontaneously without any reducing agents and encapsulated the Au NP core completely. The amount of the deposited Pd, which was proportional to the Pd precursor concentration, was associated with a decreased Au amount in the NPs, suggesting GRR-like mechanism. RDE voltammetry results verified the high catalytic activity of AuPd(1:0.61)/C and AuPd(1:0.73)/C catalysts toward ORR. Indeed, AuPd(1:0.61)/C, despite smaller Pd content than AuPd(1:0.73)/C, exhibited the best ORR activity among the catalysts examined including commercial Pt/C: positive ORR onset and $E_{1/2}$ potentials, greater limiting current density, higher n value (~4), and steeper RDE curve slope in the mixed kinetic-diffusion controlled region. This indicates that 0.61 is close to the optimal Pd/Au wt% ratio for the ORR activity of AuPd/C, presumably due to most efficient porosity of the Pd shell layer on the Au core. In addition, the sufficient stability and tolerance to methanol was also confirmed under acidic condition for the AuPd(1:0.61)/C catalyst, suggesting a possible substitute for the currently used Pt-based ORR catalyst in fuel cells.

AUTHOR INFORMATION

Corresponding Author

*Fax: + 82-2-3277-2384. E-mail: cmlee@ewha.ac.kr (C.L.), youngmilee@ewha.ac.kr (Y.L.).

Author Contributions

‡Equal contribution to this work.

ACKNOWLEDGMENT

This research was carried out under the General R/D Program of the DGIST, funded by Ministry of Education, Science and Technology (MEST) of the Republic of Korea. This work was also supported by Mid-career Researcher Program through the National Research Foundation of Korea (NRF) funded by MEST (2011-0015619).

REFERENCES

(1) Mayrhofer, K. J.; Blizanac, B. B.; Arenz, M.; Stamenkovic, V. R.; Ross, P. N.; Markovic, N. M. *J. Phys. Chem. B* **2005**, *109*, 14433–14440.
(2) Zhang, S.; Shao, Y.; Yin, G.; Lin, Y. *J. Mater Chem.* **2009**, *19*, 7995–8001.
(3) Su, F.; Tian, Z.; Poh, C. K.; Wang, Z.; Lim, S. H.; Liu, Z.; Lin, J. *Chem. Mater.* **2010**, *22*, 832–839.
(4) Ghosh, T.; Vukmirovic, M. B.; DiSalvo, F. J.; Adzic, R. R. *J. Am. Chem. Soc.* **2010**, *132*, 906–907.
(5) Lim, B.; Jiang, M.; Camargo, P. H. C.; Cho, E. C.; Tao, J.; Lu, X.; Zhu, Y.; Xia, Y. *Science* **2009**, *324*, 1302–1305.
(6) Shao, M.-H.; Sasaki, K.; Adzic, R. R. *J. Am. Chem. Soc.* **2006**, *128*, 3526–3527.
(7) Jiang, L.; Hsu, A.; Chu, D.; Chen, R. *Electrochim. Acta* **2010**, *55*, 4506–4511.
(8) Gong, K.; Du, F.; Xia, Z.; Durstock, M.; Dai, L. *Science* **2009**, *323*, 760–764.
(9) Chen, Z.; Higgins, D.; Tao, H.; Hsu, R. S.; Chen, Z. *J. Phys. Chem. C* **2009**, *113*, 21008–21013.
(10) Kongkanand, A.; Kuwabata, S.; Girishkumar, G.; Kamat, P. *Langmuir* **2006**, *22*, 2392–2396.
(11) Hammer, B.; Norskov, J. K. *Nature* **1995**, *376*, 238–240.
(12) Bond, G. C. *Catal. Today* **2002**, *72*, 5–9.
(13) Davis, R. J. *Science* **2003**, *301*, 926–927.
(14) Maye, M. M.; Kariuki, N. N.; Luo, J.; Han, L.; Njoki, P.; Wang, L.; Lin, Y.; Naslund, H. R.; Zhong, C.-J. *Gold Bull.* **2004**, *37*, 217–223.

(15) Luo; Njoki, P. N.; Lin, Y.; Wang, L.; Zhong, C. J. *Electrochem. Commun.* **2006**, *8*, 581–587.
(16) Luo, J.; Maye, M. M.; Kariuki, N. N.; Wang, L.; Njoki, P.; Lin, Y.; Schadt, M.; Naslund, H. R.; Zhong, C.-J. *Catal. Today* **2005**, *99*, 291–297.
(17) Luo, J.; Njoki, P. N.; Lin, Y.; Mott, D.; Wang, L.; Zhong, C.-J. *Langmuir* **2006**, *22*, 2892–2898.
(18) Zhang, Y.; Huang, Q.; Zou, Z.; Yang, J.; Vogel, W.; Yang, H. *J. Phys. Chem. C* **2010**, *114*, 6860–6868.
(19) Kim, S.; Jung, C.; Kim, J.; Rhee, C. K.; Choi, S.-M.; Lim, T.-H. *Langmuir* **2010**, *26*, 4497–4505.
(20) Guo, S.; Fang, Y.; Dong, S.; Wang, E. *J. Phys. Chem. C* **2007**, *111*, 17104–17109.
(21) Antolini, E. *Energy Environ. Sci.* **2009**, *2*, 915–931.
(22) Kiani, A.; Fard, E. N. *Electrochim. Acta* **2009**, *54*, 7254–7259.
(23) Lang, X. Y.; Guo, H.; Chen, L. Y.; Kudo, A.; Yu, J. S.; Zhang, W.; Inoue, A.; Chen, M. W. *J. Phys. Chem. C* **2010**, *114*, 2600–2603.
(24) Zhu, L. D.; Zhao, T. S.; Xu, J. B.; Liang, Z. X. *J. Power Sources* **2009**, *187*, 80–84.
(25) Liu, Z.; Zhao, B.; Guo, C.; Sun, Y.; Xu, F.; Yang, H.; Li, Z. *J. Phys. Chem. C* **2009**, *113*, 16766–16771.
(26) Burke, L. D.; Casey, J. K. *J. Electrochem. Soc.* **1993**, *140*, 1284–1291.
(27) Lim, B.; Kobayashi, H.; Yu, T.; Wang, J.; Kim, M. J.; Li, Z-.Y.; Rycenga, M.; Xia, Y. *J. Am. Chem. Soc.* **2010**, *132*, 2506–2507.
(28) McFarland, A. D.; Haynes, C. L.; Mirkin, C. A.; Van Duyne, R. P.; Godwin, H. A. *J. Chem. Educ.* **2004**, *81*, 544A–544B.
(29) Bard, A. J.; Parsons, R.; Jordan, J. *Standard Potentials in Aqueous Solutions*; Marcel Dekker: New York, 1985.
(30) Hameline, A.; Bellier, J. P. *J. Electroanal. Chem.* **1973**, *41*, 179–192.
(31) Zhang, H; Jin, M.; Wang, J.; Li, W.; Camargo, P. H. C.; Kim, M. J.; Yang, D.; Xie, Z.; Xia, Y. *J. Am. Chem. Soc.* **2011**, *133*, 6078–6089.
(32) Lim, B.; Jiang, M.; Camargo, P. H. C.; Cho, E. C.; Tao, J.; Lu, X.; Zhu, Y.; Xia, Y. *Science* **2009**, *324*, 1302–1305.
(33) Shim, J. H.; Kim, J.; Lee, C.; Lee, Y. *J. Phys. Chem. C* **2011**, *115*, 305–309.
(34) Hernandez, F.; Baltruschat, H. *Langmuir* **2006**, *22*, 4877–4884.
(35) McCrory, C. C. L.; Ottenwaelder, X.; Stack, T. D. P.; Chidsey, C. E. D. *J. Phys. Chem. A* **2007**, *111*, 12641–12650.
(36) McCrory, C. C. L.; Devadoss, A.; Ottenwaelder, X.; Lowe, R. D.; Stack, T. D. P.; Chidsey, C. E. D. *J. Am. Chem. Soc.* **2011**, *133*, 3696–3699.
(37) Anson, F. C.; Shi, C.; Steiger, B. *Acc. Chem. Res.* **1997**, *30*, 438–444.
(38) Koutecky, J.; Levich, V. G. *Zh. Fiz. Khim.* **1958**, *32*, 1565–1575.
(39) Treimer, S.; Tang, A.; Johnson, D. C. *Electroanalysis* **2002**, *14*, 165–171.
(40) Hsueh, K.-L.; Chin, D.-T.; Srinivasan, S. *J. Electroanal. Chem.* **1983**, *153*, 79–95.
(41) Martínez-Casillas, D. C.; Vázquez-Huerta, G.; Pérez-Robles, J. F.; Solorza-Feria, O. *J. Power Sources* **2011**, *196*, 4468–4474.
(42) Erikson, H.; Sarapuu, A.; Tammeveski, K.; Solla-Gullón, J.; Feliu, J. M. *Electrochem. Commun.* **2011**, *13*, 734–737.
(43) Sarkar, A.; Manthiram, A. *J. Phys. Chem. C* **2010**, *114*, 4725–4732.
(44) Shao, M. H.; Huang, T.; Liu, P.; Zhang, J.; Sasaki, K.; Vukmirovic, M. B.; Adzic, R. R. *Langmuir* **2006**, *22*, 10409–10415.
(45) Xiao, L.; Zhuang, L.; Liu, Y.; Lu, J.; Abruna, H. D. *J. Am. Chem. Soc.* **2008**, *131*, 602–608.
(46) Zhu, Y.; Uchida, H.; Yajima, T.; Watanabe, M. *Langmuir* **2001**, *17*, 146–154.